JOURNAL OF SPACECRAFT AND ROCKETS
Vol. 30, No. 4, July–August 1993

Thermally Induced Bending Vibrations of a Flexible Rolled-Up Solar Array

Earl A. Thornton* and Yool A. Kim†
University of Virginia, Charlottesville, Virginia 22903

An analytical approach for determining the thermal-structural response of a flexible rolled-up solar array due to a sudden increase in external heating is developed. Two analyses are presented: 1) an uncoupled thermal-structural analysis that assumes the heating and temperature gradients are not affected by thermally induced motions, and 2) a coupled thermal-structural analysis that includes the effects of structural deformations on heating and temperature gradients. The analytical methods identify key parameters for understanding the static and dynamic response. A stability criterion given in nondimensional parameters establishes the conditions for thermal flutter. Key parameters for thermal flutter include the ratio of thermal and structural response times, the solar inclination angle, and the system damping. Numerical calculations are presented for the solar arrays on the Hubble Space Telescope. Unstable oscillations are possible but are unlikely to have practical importance.

Nomenclature

A = boom cross sectional area, m^2
b = half spreader bar width, m
b' = half solar blanket width, m
c = boom specific heat, J/kg-K
E = boom modulus of elasticity, N/m^2
EI = boom bending stiffness, $N\text{-}m^2$
F_x = solar blanket tension, N/m
f = boom quasistatic shape, see Eq. (16), 1/N
g = solar blanket quasistatic shape, see Eq. (16), 1/N
h = boom wall thickness, m
k = boom thermal conductivity, W/m-K
L = solar array length, m
M_s = spreader bar mass, kg
M_T = thermal moment, N-m
P = boom axial compressive force, N
P_{cr} = buckling force, N
R = boom radius, m
r = mass distribution, kg/m
S_0 = solar heat flux, W/m^2
T = temperature, K
T_m = perturbation temperature, K
T_0 = initial temperature, K
T^* = steady-state perturbation temperature, K
$\bar{T}$ = average temperature, K
$\bar{T}_{ss}$ = steady-state average temperature, K
w = displacement in z direction, m
x, y, z = solar array coordinates
α = boom absorptivity
α_T = boom coefficient of thermal expansion, m/m/K
ϵ = boom emissivity
θ = solar incident angle, rad
ρ = boom density, kg/m^3
σ = Stefan-Boltzmann constant, $w/m^2\text{-}K^4$
σ_{sb} = solar blanket mass per unit area, kg/m^2
τ = thermal response time, s
ϕ = boom eigenfunction, m
ψ = solar blanket eigenfunction, m
ω = solar array natural frequency, rad/s

Subscripts

b = boom
Qs = quasistatic
s = spreader bar
sb = solar blanket

Received Sept. 15, 1992; revision received Oct. 30, 1992; accepted for publication Oct. 30, 1992.

*Professor and Director, Light Thermal Structures Center. Associate Fellow AIAA.

†Graduate Research Assistant; currently at Massachusetts Institute of Technology, Department of Aeronautics and Astronautics, 77 Massachusetts Ave., Room 37-350, Cambridge, MA 02139.

Introduction

THERMALLY induced vibrations of spacecraft appendages have been a recurrent problem for over 25 years. The vibrations typically occur on very low frequency booms or solar arrays due to sudden temperature changes at day-night or night-day transitions in the orbit. Sudden heating changes on a surface of an appendage may induce temperature gradients that generate time-dependent bending moments that deform the structure. The appendage motion typically can be resolved into two components: 1) a relatively large-amplitude, slowly developing quasistatic motion, and 2) a superimposed transient vibratory motion consisting of contributions from one or more appendage vibration modes. Since the spacecraft experiences no external forces or moments due to temperature changes, linear and angular momenta are conserved. Thus, because of an appendage deformation, the entire spacecraft dynamically responds with motions about the system mass center. These latter motions may degrade system operations by either undesirable displacements or unexpected accelerations. A recent paper by Thornton and Foster[1] traces the history of thermally induced spacecraft vibrations, discusses past research efforts, and illustrates stable and unstable vibrations.

Unstable vibrations are possible due to the interaction between structural deformations and incident heating. The deformation-heating coupling, sometimes called thermal flutter, may generate vibrations of increasing amplitudes that, in fact, have caused spacecraft to experience such large motions that they were unable to complete their intended missions. In the 1960s several satellites in the Orbiting Geophysical Observatories (OGO) series experienced such failures; see Ref. 1. Subsequently, several analysts (e.g., Refs. 2–4) studied the thermal flutter problem, and stability criteria were established for booms with thermally induced bending and/or torsional vibrations. Although stability criteria have been established for single booms modeled as beams, there have been very few published studies of thermally induced vibrations and flutter of more complex systems such as solar arrays. The purpose of this paper is to present an investigation of thermally induced vibrations and flutter of a flexible rolled-up solar array (FRUSA). The FRUSA concept is used for the Hubble Space Telescope (HST) solar arrays.

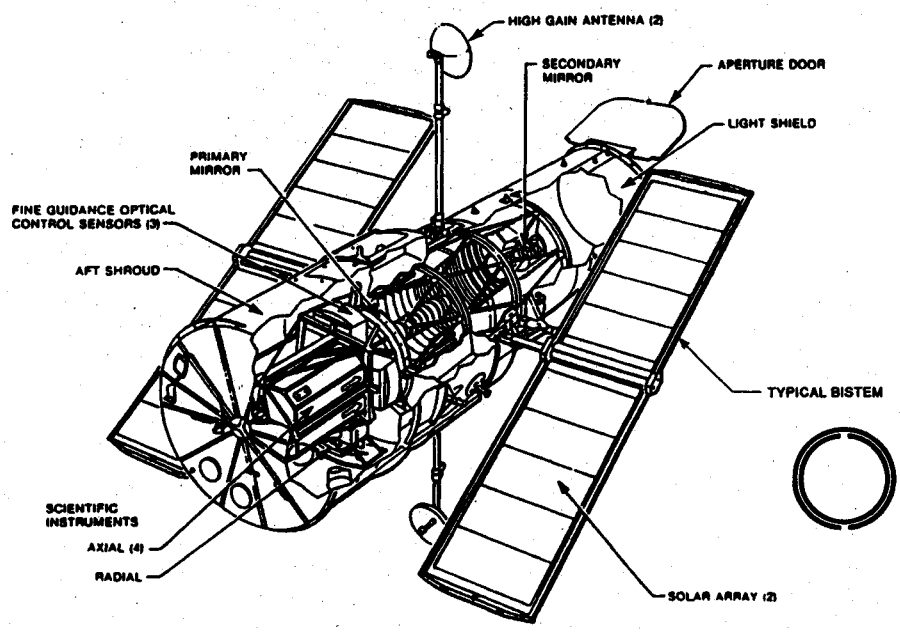

Fig. 1 Hubble Space Telescope.

The Hubble Space Telescope was launched into orbit from the Kennedy Space Center aboard the Space Shuttle Discovery on April 24, 1990. The successful deployment from the Discovery payload bay occurred one day later. The initial in-orbit checkout of spacecraft subsystems, including the discovery of the primary mirror spherical aberration, is described by Polidan.[5] During this early period another significant, long-term spacecraft problem was discovered: a pointing "jitter" induced by the thermally driven bending of the solar arrays. The solar arrays (Fig. 1) developed by the European Space Agency are the FRUSA concept designed by the Hughes Aircraft Company.

An investigation of the thermally induced solar array problem conducted at NASA Marshall Space Flight Center is described by Foster et al.[6] Pointing system data are used to develop histories of the angular motions about body-fixed coordinate axes. These histories show large-amplitude angular disturbances at the night-day and day-night transitions, followed in each case by a series of smaller disturbances. The pointing disruptions associated with these disturbances are of sufficient magnitude to compromise many of the science goals of the Hubble Space Telescope. A detailed investigation of possible excitation sources and analytical modeling of the transitional disturbance was conducted. The conclusions were that the transitional disturbances are caused primarily by thermal gradients experienced by the spacecraft booms. The series of smaller disturbances that occur between the transitional disturbances are attributed to stick/slip frictional effects in the FRUSA tensioning mechanisms.

This paper focuses on analysis of the thermal-structural response of a FRUSA for a typical night-day transition. Analytical models are used to investigate uncoupled and coupled thermal-structural dynamic responses. The study of the coupled thermal-structural response establishes a criterion for thermal flutter. Numerical results are presented for the HST solar arrays and related designs.

FRUSA Model

The HST solar array in-orbit configuration (Fig. 1) consists of two identical wings. Each wing has two flexible solar blankets that are deployed from a drum mounted on a shaft cantilevered from the spacecraft. Before deployment, the blankets and booms are furled in the drum. Each solar blanket is deployed by a rotating actuator mechanism that pushes the two rolled-up two-element storable tubular extendable member (BISTEM) booms from the drum. The BISTEM booms are connected at their deployed end by a spreader bar to which the solar blanket is attached. A BISTEM is made from thin stainless steel tapes formed into circular cross sections that are flattened and stored on spools within the drum mechanism. The stored tapes resemble a carpenter's steel tape except that, when the two tapes are deployed, they nest to form a circular cross section as shown in Fig. 1. The storage drum houses a torque mechanism that maintains blanket tension. The spreader bar houses a mechanism that compensates for slight differences in boom lengths. Thus, during orbital operations, the solar blanket experiences tension, and each BISTEM boom experiences compression.

The mathematical model and coordinate system employed in subsequent analyses are shown in Fig. 2. The model assumes 1) symmetric solar heating occurs with the solar vector parallel to the x-z plane (only flexural motions without torsion may occur); 2) the solar blanket is a membrane subjected to uniform tension in the x direction (the membrane tensile force F_x (per unit length) is assumed constant, and the membrane may experience transverse deflection that varies in the x direction, but the deformation does not vary in the y direction); 3) the right and left BISTEM booms are identical cantilevered beams, each subjected to an axial compressive force P; 4) the spreader bar is a rigid member of length $2b$ and supports the membrane tensile forces F_x over a length $2b'$; 5) the solar blanket is inextensible (solar blanket thermal expansions or contractions are neglected); and 6) the BISTEM booms are one piece, thin-walled circular tubes for determination of their temperature distributions. Equilibrium of forces on the spreader bar in the x direction requires that $P = b'F_x$. Based on these basic assumptions, analytical models will be developed for thermal and structural analyses.

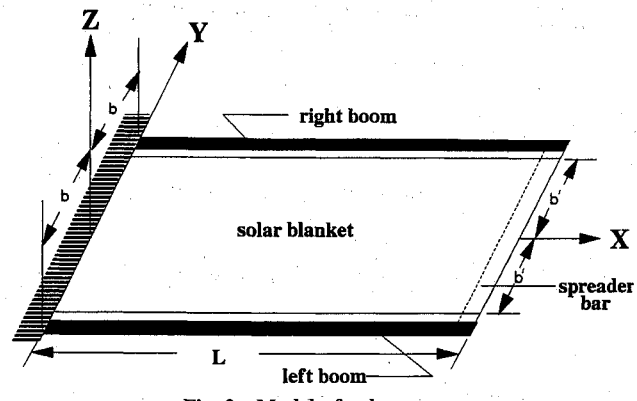

Fig. 2 Model of solar array.

Uncoupled Thermal-Structural Analyses

In uncoupled thermal-structural analyses, temperatures are computed assuming that structural motions do not affect incident, absorbed heat fluxes. That is, the temperature distribution in a boom is assumed independent of structural deformations. This assumption is consistent with classical heat transfer that assumes that mechanical systems are rigid bodies for the purpose of writing the energy conservation equation. The thermal analysis to be presented follows the approach employed previously in Refs. 3 and 4.

Thermal Analysis

The thermal model of a boom is shown in Fig. 3. The boom is subjected to an incident solar heat flux S_0 that is assumed to vary as a step function with time. Thus, for time $t<0$, the incident flux is zero, and for $t \geq 0$, the incident flux has a constant value of S_0. Earth emitted and reflected radiation heat fluxes are neglected. Thermal energy losses at the cantilevered support at $x = 0$ are neglected. Since the heat flux S_0 does not vary along the tube length, the temperature distribution at every cross section is the same. The tube wall thickness h is assumed small in comparison with the tube radius R, $h \ll R$, and the temperature is assumed constant through the tube wall thickness. Thus the temperature T varies only with the angular coordinate ϕ and time t, $T(\phi, t)$. Thermal energy is emitted from the tube's external surface, assuming diffuse radiation, but internal radiation within the tube is neglected. All thermal properties are assumed constant. With these assumptions, conservation of energy yields

$$\frac{\partial T}{\partial t} - \frac{k}{\rho c R^2}\frac{\partial^2 T}{\partial \phi^2} + \frac{\sigma \epsilon}{\rho c h} T^4 = \frac{\alpha S_0}{\rho c h}\delta \cos \phi \tag{1}$$

The parameter δ is employed to indicate that only one side of the tube is heated,

$$\delta = 1 \qquad -\pi/2 < \phi < \pi/2$$

$$\delta = 0 \qquad \pi/2 < \phi < 3\pi/2$$

The initial condition is $T(\phi, 0) = T_0$, and the only boundary condition is that the temperature distribution is symmetrical about the x-z plane, $T(\phi, t) = T(-\phi, t)$.

To solve Eq. (1), three approximations are used. First, the temperature $T(\phi, t)$ is approximated as the sum of an average temperature $\bar{T}(t)$ and a perturbation temperature $T_m(\phi, t)\cos\phi$ that varies from the front face to the back face of the boom,

$$T(\phi, t) = \bar{T}(t) + T_m(t)\cos\phi \tag{2}$$

Second, the amplitude of the perturbation temperature is assumed to be small in comparison with the average tube temperature,

$$T_m/\bar{T} < 1$$

Third, the incident heat flux distribution is expanded as a Fourier series neglecting higher order terms,

$$\delta \cos\phi \cong (1/\pi) + \tfrac{1}{2}\cos\phi$$

With these approximations, Eq. (2), when substituted into Eq. (1), yields two uncoupled ordinary differential equations,

$$\frac{d\bar{T}}{dt} + \frac{\sigma\epsilon}{\rho c h}\bar{T}^4 = \frac{1}{\pi}\frac{\alpha S_0}{\rho c h} \tag{3a}$$

$$\frac{dT_m}{dt} + \left(\frac{k}{\rho c R^2} + \frac{4\sigma\epsilon}{\rho c h}\bar{T}^3\right)T_m = \frac{1}{2}\frac{\alpha S_0}{\rho c h} \tag{3b}$$

with initial conditions $\bar{T}(0) = T_0$, and $T_m(0) = 0$. At radiation equilibrium, Eq. (3a) shows that the steady-state average tube temperature is

$$\bar{T}_{ss} = \left(\frac{1}{\pi}\frac{\alpha S_0}{\sigma\epsilon}\right)^{1/4} \tag{4}$$

Equation (3a) can be integrated directly by separation of variables. After imposing the initial condition the result may be written as

$$\frac{1}{4\bar{T}_{ss}^3}\left[\ell n\frac{(\bar{T}_{ss} - \bar{T})(\bar{T}_{ss} + T_0)}{(\bar{T}_{ss} + \bar{T})(\bar{T}_{ss} - T_0)} + 2\tan^{-1}\frac{T_0}{\bar{T}_{ss}} - 2\tan^{-1}\frac{\bar{T}}{\bar{T}_{ss}}\right] + \frac{\sigma\epsilon}{\rho c h}t = 0 \tag{5}$$

Equation (5) is a transcendental equation that implicitly defines $\bar{T}(t)$. To compute the average temperature for a given t, the equation is solved numerically.

The perturbation temperature T_m cannot be obtained analytically because of the presence of the term $\bar{T}^3$ on the left-hand side of Eq. (3b). However, numerical studies show that this term may be assumed constant for some tubes. Assuming that $\bar{T}^3$ may be approximated as $\bar{T}_{ss}^3$ produces a linear differential equation that may be written as

$$\frac{dT_m}{dt} + \frac{1}{\tau}T_m = \frac{1}{2}\frac{\alpha S_0}{\rho c h} \tag{6a}$$

where

$$\frac{1}{\tau} = \frac{k}{\rho c R^2} + \frac{4\sigma\epsilon\bar{T}_{ss}^3}{\rho c h} \tag{6b}$$

The solution for the perturbation temperature may then be written as

$$T_m = T^*(1 - e^{-t/\tau}) \tag{7a}$$

where

$$T^* = \frac{1}{2}\frac{\alpha S_0}{\rho c h}\tau \tag{7b}$$

The temperature T^* is the steady-state value of the perturbation temperature.

The temperature distribution at a boom cross section can be evaluated from Eq. (2) using the average temperature $\bar{T}(t)$ from Eq. (5), and the perturbation temperature $T_m(t)$ from

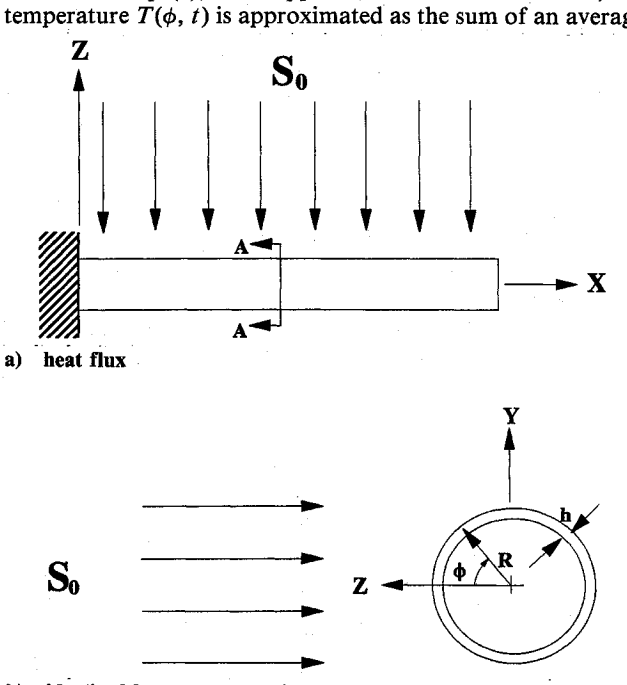

Fig. 3 Uncoupled thermal model of solar array boom.

Eq. (7). The $T_m(t)\cos\phi$ term in Eq. (2) represents the tube temperature gradient from the heated to the unheated side. This temperature gradient induces a thermal bending moment that causes a boom to bend.

Structural Analysis

The structural analysis is performed using equations of motion for the booms, the solar blanket, and the spreader bar. The equations are solved subject to boundary conditions at the cantilevered support and interface conditions at the spreader bar. As a result of symmetry, the two booms' motions are synchronous, and only one boom needs to be considered.

The equation of motion for a boom is

$$EI\frac{\partial^4 w_b}{\partial x^4} + P\frac{\partial^2 w_b}{\partial x^2} + \frac{\partial^2 M_T}{\partial x^2} + \rho A\frac{\partial^2 w_b}{\partial t^2} = 0 \tag{8a}$$

where w_b is the boom deflection, I is the cross-sectional moment of inertia, and M_T is defined by

$$M_T = \int_A E\alpha_T \Delta T z \, dA \tag{8b}$$

where α_T is the coefficient of thermal expansion, and $\Delta T(\phi, t)$ denotes a beam's cross-sectional temperature gradient. The equation of motion of the solar blanket is

$$F_x\frac{\partial^2 w_{sb}}{\partial x^2} = \sigma_{sb}\frac{\partial^2 w_{sb}}{\partial t^2} \tag{9}$$

where $w_{sb}(x, t)$ is the solar blanket deflection. The equation of motion of the spreader bar is

$$2V_Z(L, t) + \int_{-b'}^{b'} F_x\frac{\partial w_{sb}}{\partial x}(L, t)\, dy + M_s\frac{d^2 w_s}{dt^2} = 0 \tag{10a}$$

where V_Z is the boom shear force defined by

$$V_Z = -EI\frac{\partial^3 w_b}{\partial x^3} - P\frac{\partial w_b}{\partial x} - \frac{\partial M_T}{\partial x} \tag{10b}$$

In Eq. (10a), $w_s(t)$ is the spreader bar deflection, and M_s is the spreader bar mass.

The boom boundary conditions are

$$\begin{gathered} w_b(0, t) = 0 \\ \frac{\partial w_b}{\partial x}(0, t) = 0 \\ M_y(L, t) = 0 \end{gathered} \tag{11a}$$

where M_y is the boom bending moment defined by

$$M_y = -EI\frac{\partial^2 w_b}{\partial x^2} - M_T \tag{11b}$$

The solar blanket boundary conditions are

$$\begin{gathered} w_{sb}(0, t) = 0 \\ w_{sb}(L, t) = w_b(L, t) = w_s(t) \end{gathered} \tag{11c}$$

The initial conditions are that the displacements and velocities at $t = 0$ are zero. Equations (8–11) formulate the thermal-structural boundary/initial value problem. The solution is described in terms of: 1) the buckling modes, 2) the free vibration frequencies and modes, and 3) a modal expansion for the dynamic response.

Boom Buckling

Since the booms are subjected to compressive forces P, buckling may occur. Critical buckling modes are determined by solving Eq. (8a) subject to the boom boundary conditions assuming static behavior and neglecting thermal effects. The result is

$$P_{cr} = n^2\frac{\pi^2 EI}{L^2} \qquad n = 1, 2, 3, \ldots \tag{12}$$

where P_{cr} denotes Euler buckling loads. The result is identical to that of a pinned-end beam column. This agreement occurs because the line of action of the compressive force P passes through the end supports of the boom as in the case of a simply supported beam.

Vibration Modes

Vibration frequencies and mode shapes are determined by solving Eqs. (8–10) subject to the boundary conditions assuming harmonic motion and neglecting thermal effects. Assuming

$$\begin{gathered} w_b = \phi(x)\sin\omega t \\ w_{sb} = \psi(x)\sin\omega t \end{gathered}$$

where $\phi(x)$ and $\psi(x)$ are the eigenfunctions, the analysis yields

$$\phi(x) = \frac{D_1}{D_2}\sin\delta x - \cos\delta x - \frac{D_1}{D_2}\frac{\delta}{\epsilon}\sinh\epsilon x + \cosh\epsilon x \tag{13a}$$

$$\psi(x) = \phi(L)\sin\left(\sqrt{\frac{\sigma_{sb}}{F_x}}\,\omega x\right)\Big/\sin\left(\sqrt{\frac{\sigma_{sb}}{F_x}}\,\omega L\right) \tag{13b}$$

where

$$\begin{gathered} D_1 = \delta^2\cos\delta L + \epsilon^2\cosh\epsilon L \\ D_2 = \delta^2\sin\delta L + \delta\epsilon\sinh\epsilon L \end{gathered} \tag{13c}$$

and

$$\begin{gathered} \delta = \left\{\frac{P}{2EI}\left[\left(1 + \frac{4\rho A\omega^2 EI}{P^2}\right)^{1/2} + 1\right]\right\}^{1/2} \\ \epsilon = \left\{\frac{P}{2EI}\left[\left(1 + \frac{4\rho A\omega^2 EI}{P^2}\right)^{1/2} - 1\right]\right\}^{1/2} \end{gathered} \tag{13d}$$

For free vibrations the frequency equation is derived by substituting Eqs. (13) into Eqs. (10),

$$EI\phi'''(L) + P\phi'(L) - P\psi'(L) + \tfrac{1}{2}M_s\omega^2\phi(L) = 0 \tag{14}$$

where a prime superscript denotes differentiation with respect to x. For a given column force P, Eq. (14) is solved numerically to obtain the natural frequencies.

Dynamic Response

A modal analysis procedure for determining thermally induced vibrations of a beam was developed originally in Ref. 7. The same basic approach is followed here for the solar array, but details differ and a more complex orthogonality condition is required. The thermally induced dynamic response can be viewed as the sum of a quasistatic deflection of the array and vibrations about the quasistatic deflection. The response for a boom or solar blanket can be written as

$$w(x, t) = w_{Qs}(x, t) + \tilde{w}(x, t) \tag{15}$$

where w_{Qs} is the quasistatic response, and $\tilde{w}$ is the vibration response. The quasistatic responses for a boom and the solar

blanket are represented as

$$w_{bQs}(x, t) = M_T(t)f(x)$$
$$w_{sbQs}(x, t) = M_T(t)g(x) \tag{16}$$

where $M_T(t)$ is the thermal moment, and $f(x)$ and $g(x)$ are the quasistatic deflected shapes. From Eq. (8b) the thermal moment may be evaluated using the temperature gradient term from Eq. (2). With these substitutions, the integral is evaluated over the tube cross section shown in Fig. (3). Thus

$$M_T(t) = \frac{EI\alpha_T T_m(t)}{R} \tag{17}$$

where for a thin tube $I = \pi hR^3$, and $T_m(t)$ is given by Eq. (7). Note that, due to sudden boom heating, the thermal bending moment monotonically increases, approaching a steady-state value for large values of time.

For the quasistatic response, the inertia forces in the equations of motion, Eqs. (8–10), are neglected. Solving these equations with the boundary conditions yields

$$w_{bQs}(x, t) = \frac{M_T(t)}{P}\left[\cos \lambda x - 1 + \frac{(\cos \lambda L - 1)}{\sin \lambda L} \times (\lambda x - \sin \lambda x)\right] \tag{18a}$$

where $\lambda^2 = P/EI$ and

$$w_{SbQs}(x, t) = \frac{M_T(t)}{P}\left[\frac{\lambda(\cos \lambda L - 1)}{\sin \lambda L}x\right] \tag{18b}$$

Since the thermal moment monotonically increases to a steady-state value, the quasistatic deflections do likewise. The steady-state deflected positions of the booms and solar blanket are maintained as long as the solar flux is applied.

Modal expansions of the quasistatic response are used to obtain the dynamic response. The functions of x defined by Eqs. (16) and (18) are represented by

$$f(x) = \sum_{n=1}^{\infty} a_n \phi_n(x) \tag{19a}$$

$$g(x) = \sum_{n=1}^{\infty} a_n \psi_n(x) \tag{19b}$$

where $\phi_n(x)$ and $\psi_n(x)$ are the eigenfunctions given in Eqs. (13). The coefficients are evaluated using the orthogonality condition

$$\int_0^L r_b(x)\phi_n(x)\phi_m(x)\,dx + \int_0^\ell r_{sb}(x)\psi_m(x)\psi_n(x)\,dx = 0 \qquad m \neq n \tag{20}$$

where the weighting functions $r_b(x)$ and $r_{sb}(x)$ are the mass distributions for the booms and solar blankets, respectively,

$$r_b(x) = \rho A + \tfrac{1}{2}M_s\delta(x - L)$$
$$r_s(x) = \sigma_{sb}b'$$

where $\delta(x - L) = 0$ for $0 < x < L$, and $\delta(x - L) = 1$ for $x = L$. With the orthogonality condition, the coefficients of the expansions a_n can be evaluated in the usual way:

$$a_n = \frac{\rho A\int_0^L \phi_n(x)f(x)\,dx + b'\sigma_{sb}\int_0^L \psi_n(x)g(x)\,dx + (M_s/2)\phi_n(L)f(L)}{\rho A\int_0^L \phi_n^2(x)\,dx + b'\sigma_{sb}\int_0^L \psi_n^2(x)\,dx + (M_s/2)\phi_n^2(L)}$$

The expression for a_n shows that all elements of the solar array, i.e., the boom, the solar blanket, and the spreader bar, affect the modal expansion of the quasistatic shapes. The dynamic response of a boom is then represented, based on Eqs. (15) and (16), as

$$w_b(x, t) = M_T(t)\sum_{n=1}^{\infty} a_n\phi_n(x) + \sum_{n=1}^{\infty} \phi_n(x)T_n(t)$$

and the time functions $T_n(t)$ are evaluated using standard separation of variable techniques. The solar blanket deflection is represented similarly. The final solutions for the dynamic response are

$$w_b(x, t) = M_T(t)f(x) + \frac{\alpha_T T^* EI}{R}\sum_{n=1}^{\infty}\frac{a_n\phi_n(x)}{1 + \omega_n^2\tau^2}\bar{T}_n(t) \tag{21a}$$

$$w_{sb}(x, t) = M_T(t)g(x) + \frac{\alpha_T T^* EI}{R}\sum_{n=1}^{\infty}\frac{a_n\psi_n(x)}{1 + \omega_n^2\tau^2}\bar{T}_n(t) \tag{21b}$$

where a new time function has been introduced defined by

$$\bar{T}_n(t) = e^{-t/\tau} - \omega_n\tau \sin \omega_n t - \cos \omega_n t \tag{22}$$

As mentioned previously, the dynamic response consists of the nonoscillatory quasistatic response represented by the first term in Eq. (21) plus the vibratory response represented by the second term. In this analysis, damping has been neglected so that the vibratory terms persist for large time. If damping were included, the vibratory terms diminish with increasing time so that the solar array deflected shape would approach the quasistatic shape. A key parameter that determines the relative magnitude of thermally induced vibrations is the product $\omega_n\tau$. From Eqs. (6) and (7), τ can be seen as a measure of the thermal response time. Writing ω_n in terms of a modal natural period shows that $\omega_n\tau$ represents the ratio of the thermal response time to the structural response time. When $\omega_n\tau$ is of the order of unity, thermally induced oscillations become large.

Coupled Thermal-Structural Analyses

In the preceding section uncoupled thermal-structural analyses were presented based on the assumption that the absorbed heat flux was not affected by the boom's deformations. In this section the effect of the boom's deformation is taken into account, and the thermal-structural analyses are coupled.

Thermal Analysis

A deformed boom with the incident heat flux vector S_0 is shown in Fig. 4. To provide generality, the heat flux vector is inclined to the vertical by the angle θ. In writing the energy conservation equation, the heat flux absorbed by the tube is the component normal to the surface. Because of bending, a normal to the beam surface has rotated through a small angle equal to the beam slope. Thus the incident normal heat flux to the surface varies with x along the beam and can be expressed by

$$S = S_0\cos\left(\theta - \frac{\partial w_b}{\partial x}\right) \tag{23}$$

Then the conservation of energy equation, Eq. (1), becomes

$$\frac{\partial T}{\partial t} - \frac{k}{\rho cR^2}\frac{\partial^2 T}{\partial \phi^2} + \frac{\sigma\epsilon}{\rho ch}T^4 = \frac{\alpha S_0}{\rho ch}\delta \cos \phi \cos\left(\theta - \frac{\partial w_b}{\partial x}\right) \tag{24}$$

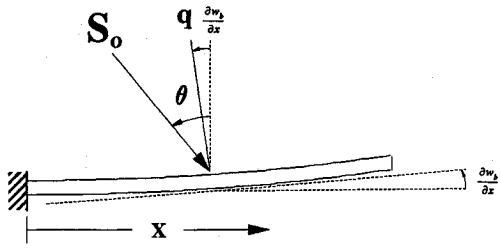

Fig. 4 Heat flux for coupled thermal-structural analysis.

Because the absorbed energy depends on the beam slope, the temperature varies along the beam length. The approximate solution for the temperature, Eq. (2), now takes the form

$$T(x,\ \phi,\ t) = \bar{T}(x,\ t) + T_m(x,\ t)\cos\phi \tag{25}$$

where all temperatures depend on x. Proceeding with the same approximations as before produces two similar differential equations,

$$\frac{\partial \bar{T}}{\partial t} + \frac{\sigma\epsilon}{\rho c h}\bar{T}^4 = \frac{1}{\pi}\frac{\alpha S_0}{\rho c h}\cos\left(\theta - \frac{\partial w_b}{\partial x}\right) \tag{26a}$$

$$\frac{\partial T_m}{\partial t} + \frac{1}{\tau}T_m = \frac{1}{2}\frac{\alpha S_0}{\rho c h}\cos\left(\theta - \frac{\partial w_b}{\partial x}\right) \tag{26b}$$

At steady state, the incident heat flux approaches a constant value that is approximated by neglecting the boom slope. The steady-state average temperature is then found from Eq. (26a) as

$$\bar{T}_{ss} = \left(\frac{1}{\pi}\frac{\alpha S_0 \cos\theta}{\sigma\epsilon}\right)^{1/4} \tag{27}$$

An approximate perturbation temperature function was obtained previously by assuming τ to be constant; see Eq. (6b). Based on this assumption, Eq. (26b) can be solved to yield

$$T_m(x,\ t) = \frac{e^{-t/\tau}T^*}{\tau}\int_0^t e^{p/\tau}\cos\left(\theta - \frac{\partial w_b}{\partial x}\right)dp \tag{28}$$

The thermal moment can then be obtained from Eq. (8b),

$$M_T(x,\ t) = \frac{EI\alpha_T T^*}{R\tau}e^{-t/\tau}\int_0^t e^{p/\tau}\cos\left(\theta - \frac{\partial w_b}{\partial x}\right)dp \tag{29}$$

Structural Analysis

The thermal-structural boundary/initial value problem was formulated in Eqs. (8–11). Because of the dependence of the thermal moment on the beam slope that appears in the integrand of Eq. (29), a modal representation of the response could not be obtained. Instead, an approximate solution based on the method of weighted residuals (MWR) was developed.

Approximate Solution

The solutions for the boom deflection and the solar blanket are taken in the form

$$\begin{aligned} w_b(x,\ t) &= N_b(x)U(t) \\ w_{sb}(x,\ t) &= N_{sb}(x)U(t) \end{aligned} \tag{30}$$

where the approximating functions N_b and N_{sb} are assumed to satisfy the conditions

$$N_b(0) = 0$$

$$N_b'(0) = 0$$

$$N_{sb}(0) = 0$$

$$N_{sb}(L) = N_b(L)$$

These functions are nondimensional to allow the time function $U(t)$ to represent the deflection of the array end as a function of time. The method of weighted residuals is based on

$$\int_0^L R(x,\ t)W(x)\ dx = 0 \tag{31}$$

where $R(x, t)$ is the residual from substituting an approximate solution such as Eq. (30) in a differential equation, and $W(x)$ is a weighting function. Using Galerkin's form of MWR, the weighting functions are selected as the approximating functions. Thus, for the boom, Eq. (8a) can be written as

$$\int_0^L \left(EI\frac{\partial^4 w_b}{\partial x^4} + P\frac{\partial^2 w_b}{\partial x^2} + \frac{\partial^2 M_T}{\partial x^2} + \rho A\frac{\partial^2 w_b}{\partial t^2}\right)N_b(x)\ dx = 0 \tag{32a}$$

and for the solar blanket, Eq. (9) becomes

$$\int_0^L \left(F_x\frac{\partial^2 w_{sb}}{\partial x^2} - \sigma_{sb}\frac{\partial^2 w_{sb}}{\partial t^2}\right)N_{sb}(x)\ dx = 0 \tag{32b}$$

The balance of the MWR solution consists of: 1) integrating the spatial derivatives by parts, 2) introducing the boundary conditions, and 3) introducing the approximations for w_b and w_{sb} from Eq. (30). The result is an ordinary differential equation for the unknown function $U(t)$,

$$\ddot{U} + \omega_0^2 U = F(t)/M \tag{33a}$$

where ω_0 is an approximation to the first mode natural frequency

$$\omega_0 = \sqrt{K/M} \tag{33b}$$

and

$$K = EI\int_0^L (N_b'')^2\ dx - P\int_0^L (N_b')^2\ dx + P\int_0^L (N_{sb}')^2\ dx \tag{33c}$$

$$M = \rho A\int_0^L N_b^2\ dx + \sigma_{sb}'\int_0^L N_{sb}^2\ dx + \tfrac{1}{2}M_s N_b^2(L) \tag{33d}$$

$$F(t) = -\int_0^L N_b'' M_T(x,\ t)\ dx \tag{33e}$$

where K, M, and F are the stiffness, mass, and force, respectively, for the equivalent single degree of freedom (SDOF) system defined by Eq. (33a). The equivalent SDOF remains difficult to solve analytically because the thermal moment appearing in Eq. (33e) contains the unknown function $U(t)$ inside of an integral as shown in Eq. (29). However, with Laplace transforms, a solution may be obtained. First, the stability of the solution will be investigated and a stability criterion established.

Stability Criterion

The stability of the dynamic response is determined by obtaining the Laplace transform of the differential equation of motion and applying the Routh-Hurwitz criterion. With damping and substitution for the thermal moment using Eq. (29), the equation of motion becomes

$$\ddot{U} + 2\zeta\omega_0\dot{U} + \omega_0^2 U = F(t)/M \tag{34a}$$

$$F(t) = \frac{-EI\alpha_T T^*}{R\tau}e^{-t/\tau}\int_0^L\int_0^t N_b''(x)e^{p/\tau}\cos\left(\theta - \frac{\partial w_b}{\partial x}\right)dp \tag{34b}$$

where ζ is the damping ratio. Because of the coupling between the structural and the thermal response, which is represented by the cosine term in the expression for the thermal moment in Eq. (29), Eq. (34a) is nonlinear and difficult to solve analytically. However, Eq. (34a) can be linearized by approximating

the cosine term based on the assumption that the boom's slope is small,

$$\cos\left(\theta - \frac{\partial w_b}{\partial x}\right) = \cos\theta + \frac{\partial w_b}{\partial x}\sin\theta$$

Thus the applied load is approximated by

$$F(t) = \frac{-EI\alpha_T T^*}{R\tau} e^{-t/\tau}\int_0^L \int_0^t N_b''(x) e^{p/\tau}[\cos\theta + N_b'(x)U(p)\sin\theta]\,dp$$

After the Laplace transform, the transfer function is defined as

$$\frac{U(s)}{G(s)} = \frac{1/M}{q(s)} \tag{35a}$$

where the input $G(s)$ is

$$G(s) = \frac{-EI\alpha_T T^*\cos\theta \int_0^L N_b''(x)\,dx}{R\tau}\frac{1}{s} \tag{35b}$$

The characteristic equation $q(s)$, which determines the stability of the solution, is

$$q(s) = s^3 + \left(2\zeta\omega_0 + \frac{1}{\tau}\right)s^2 + \left(\omega_0^2 + \frac{2\zeta\omega_0}{\tau}\right)s + \frac{\omega_0^2}{\tau} + \frac{EI\alpha_T T^*\sin\theta}{\tau MR}\int_0^L N_b''(x)N_b'(x)\,dx \tag{36}$$

The transfer function can be nondimensionalized to obtain a dimensionless characteristic equation to permit an effective parameter study. A dimensionless $q(s)$ can be written as

$$\bar{q}(s) = \bar{s}^3 + (2\zeta + \kappa)\bar{s}^2 + (1 + 2\zeta\kappa)\bar{s} + (\kappa + \kappa\eta) \tag{37a}$$

where

$$\bar{s} = s/\omega_0 \tag{37b}$$

$$\kappa = 1/\omega_0\tau \tag{37c}$$

$$\eta = \alpha_T T^*(B/R)\sin\theta \tag{37d}$$

$$B = \frac{EI\int_0^L N_b''(x)N_b'(x)\,dx}{K} \tag{37e}$$

In the last equation, K is the stiffness by Eq. (33c). For a stable response, the Routh-Hurwitz test requires that

$$\eta < \frac{2\zeta\kappa^2 + 4\zeta^2\kappa + 2\zeta}{\kappa} \tag{38}$$

Equation (38) indicates that the stability of the response becomes critical when η is equal to the right-hand side of the equation,

$$\eta_{cr} = \frac{2\zeta\kappa^2 + 4\zeta^2\kappa + 2\zeta}{\kappa} \tag{39}$$

These critical values represent the boundaries between stable and unstable responses. Thus, for stability, η must be less than the critical value. Because ζ and κ are positive quantities, η_{cr} is always positive. However, negative and zero incident angles, $\theta \le 0$ yield $\eta \le 0$, and thus η is always less than η_{cr} for these solar heating orientations. Thus, the stability criterion shows that negative and zero incident angles always produce stable responses. However, for $\theta > 0$, the coupled thermal-structural vibrations may be unstable, i.e., thermal flutter may occur.

Dynamic Response

The dynamic response is obtained by inversion of the Laplace transform of $U(s)$ given in Eq. (35) to obtain $U(t)$. Then approximate solutions for $w_b(x, t)$ and $w_{sb}(x, t)$ are given by Eq. (30). Finally, the perturbation temperature $T_m(x, t)$ can be determined by Eq. (28). These steps were performed numerically and will be described in the next section.

Table 1 Hubble Space Telescope solar array data

Parameter	Value
α	0.5
α_T, m/m/K	1.692E-5
S_0, W/m^2	1.350E + 3
σ, W/m^2-K^4	5.670E-8
ϵ	0.13
c, J/kg-K	5.020E + 2
ρ, kg/m^3	7.010E + 3
h, m	2.35E-4
k, W/m-K	1.661E + 1
R, m	1.092E-2
E, N/m^2	1.930E + 11
EI, N-m^2	1.711E + 2
L, m	5.91
σ_{sb}, kg/m^2	1.589
M_s, kg	1.734
b, m	1.428
b', m	1.194
A, m^2	1.613E-5
P, N	14.75

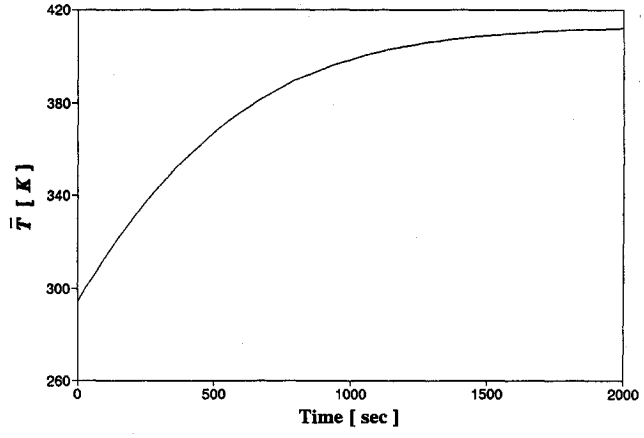

Fig. 5 Boom average temperature response.

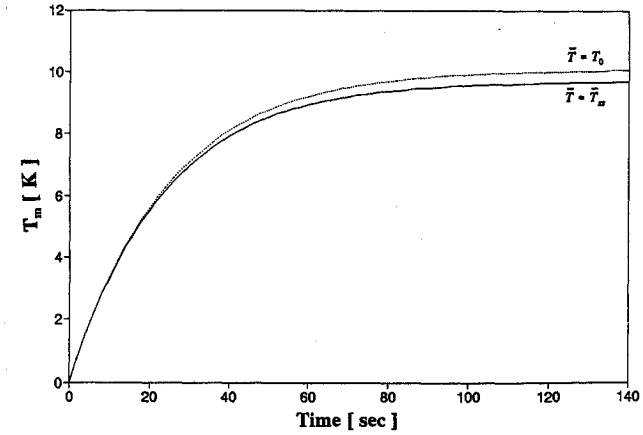

Fig. 6 Boom perturbation temperature response.

Numerical Results

The numerical calculations use data (Table 1) for the Hubble Space Telescope solar array that were obtained from Ref. 8. The tube material is stainless steel.

Uncoupled Thermal Analysis

Numerical results for predicted temperatures due to the suddenly applied heating are presented to assess the assumptions made in the analytical development and provide insight into the thermal response. Figures 5 and 6 present the predicted average temperature response, Eq. (5), and the perturbation temperature response, Eq. (7), respectively. These figures show that $T_m/\bar{T} = 0.03$, which supports the assumption made in the derivation that $T_m/\bar{T} < 1$. The perturbation temperature T_m was computed for two different values of $\bar{T}$ in the equation for τ, Eq. (6b). Although $\bar{T}$ is assumed to be $\bar{T}_{ss}$ in Eq. (6b), Fig. 6 shows that assuming $\bar{T}$ to be T_0 is also reasonable. The two curves are similar in shape, and the predicted values for $T_m(t)$ are in good agreement.

The average temperature $\bar{T}$ approaches steady-state in approximately 1500 s. In contrast, the perturbation temperature nears steady state within 120 s. The perturbation temperature rises at a much faster rate than the average temperature; hence a temperature gradient develops in the boom in a relatively short time after the boom is exposed to solar radiation.

Temperature profiles for the upper one-half of the boom cross section at various times are shown in Fig. 7. These also demonstrate the development of the boom thermal gradients. To provide further validation for the thermal analytical solution, a finite element analysis of Eq. (1) was also performed.

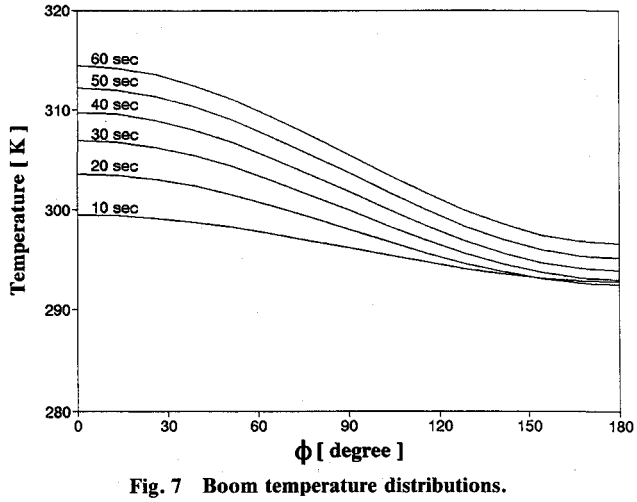

Fig. 7 Boom temperature distributions.

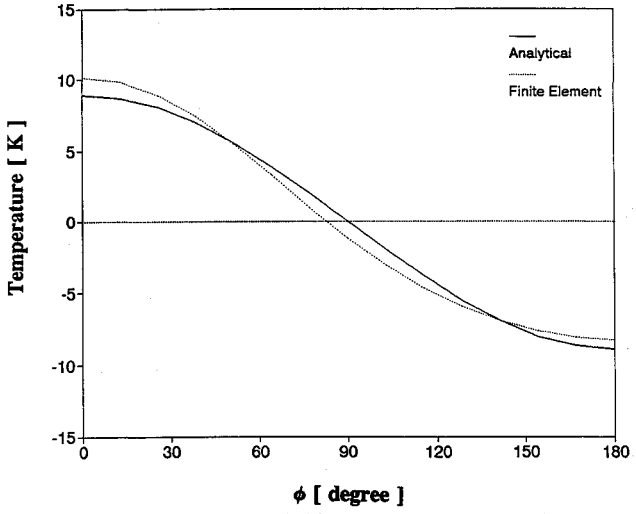

Fig. 8 Comparison of analytical and finite element predicted perturbation temperature distributions at $t = 60$ s.

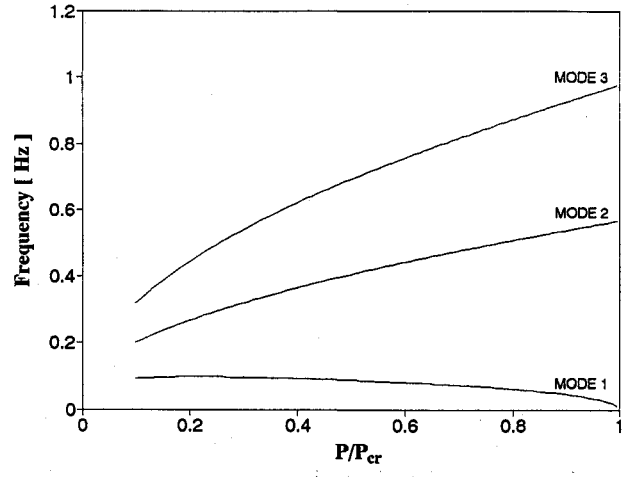

Fig. 9 Variation of modal frequencies with axial force ratio P/P_{cr}.

Figure 8 compares perturbation temperature profiles from the analytical solution and the finite element solution at $t = 60$ s. The two results are in good agreement, providing further validation for the approximations made in developing the analytical solution. This result is significant because the temperature gradient induces boom bending and thus the vibration of the solar array. The temperature gradient ΔT across a boom is $2T_m$ or about 20 K (36°F).

Uncoupled Structural Analysis

Boom Buckling

The minimum critical buckling load for a boom was computed using Eq. (12) and the data presented in Table 1. The critical buckling load is $P_{cr} = 48.3$ N. From Table 1 the nominal boom force due to the solar blanket tension is $P = 14.8$ N or 31% of P_{cr}.

Vibration Modes

The vibration frequencies were computed from Eq. (14) for various values of P/P_{cr}. The variation of the frequencies of the first three modes with P/P_{cr} is presented in Fig. 9. The frequencies are not shown for small values of P/P_{cr} since the frequency equation applies only if there is membrane tension. The figure shows that the first mode frequency decreases with increasing axial force and approaches zero as expected when $P/P_{cr} = 1$. The mode shapes and frequencies for the HST solar array are displayed in Fig. 10. Note that the frequency of the first mode is relatively small, $f_1 = 0.0967$ Hz.

Quasistatic Response

The quasistatic response of the HST solar array was computed using Eqs. (18), and the shape of the boom is shown at various times in the response in Fig. 11. The solar panel deflection varies linearly with x and is not shown. The quasistatic response develops smoothly with time and approaches a maximum deflection of $w_b(L) = -35R$ in about 120 s as the temperature gradient approaches steady state. The minus sign results because the top surfaces of the booms are heated, and the booms deflect in the negative direction in Fig. 2. Thus due to a temperature gradient $\Delta T = 20$ K, the maximum solar array deflection is predicted to be $35R = 0.38$ m (15 in.). Reference 6 predicts a temperature gradient $\Delta T = 30$ K. The present analysis underestimates the temperature gradient because a BISTEM is assumed to be a solid thin-walled tube. In Ref. 6 a finite difference thermal model was employed, and a BISTEM was modeled thermally as separate slit tubes with heat transfer between the tubes represented by a contact resistance.

Dynamic Response

The dynamic response of the HST solar array is shown in Fig. 12. The figure shows time histories of the boom tip

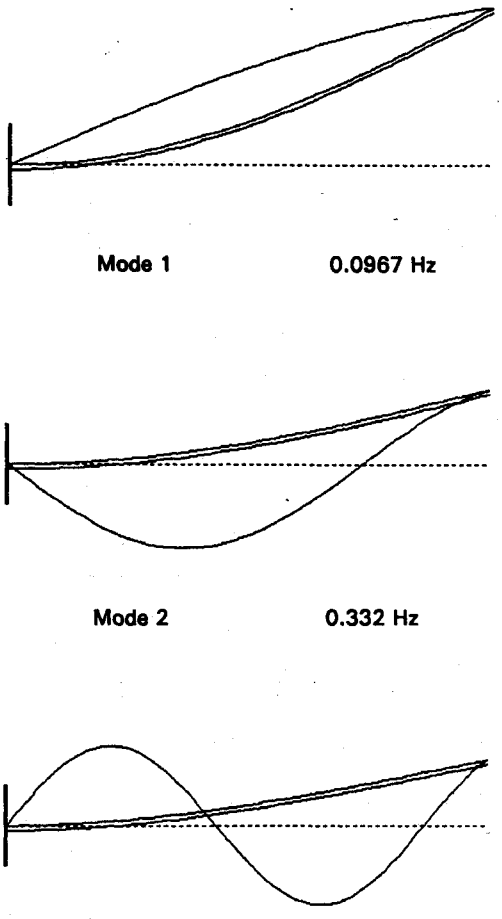

Fig. 10 First three vibration modes of HST solar array.

deflection for three ratios of P/P_{cr}. The responses consist of a thermally induced undamped oscillation superimposed on the quasistatic deflection. The responses shown use the first three modes in the modal analysis. For the ratio of $P/P_{cr} = 0.31$, the value used in the HST design, the amplitude of the oscillation is about $2.5R$ or 0.027 m (1.1 in.). Thus the amplitude of the thermally induced oscillations predicted by the uncoupled analysis are relatively small in comparison with the quasistatic deflections. The higher ratios of P/P_{cr} lower the bending stiffness and the first mode frequency of the boom and lead to larger quasistatic deflections and increased vibration amplitudes. Thus, the P/P_{cr} ratio is a critical factor in the thermally induced dynamic response of the solar arrays.

Coupled Thermal-Structural Analysis

The coupled thermal-structural analysis depends on selection of the approximating functions $N_b(x)$ and $N_{sb}(x)$ used in Eq. (30). With these functions selected, the various integrals that define parameters such as K, Eq. (33c), M, Eq. (33d), and B, Eq. (37e), may be evaluated. Several approximating functions were considered, including the quasistatic deflection shapes and the eigenfunctions from the uncoupled analysis. The eigenfunctions for the first mode were selected because these functions yielded the best approximation for the first mode frequency ω_0. For $0.1 < P/P_{cr} < 0.75$, the maximum error in the approximate frequency is less than 1%.

Stability Criterion

Using the stability criterion given in Eq. (38), the stability boundaries for the coupled thermal-structural response of the solar arrays are shown in Fig. 13. On the vertical axis of the figure is the nondimensional parameter η that is a measure of the thermally induced response since it is proportional to the coefficient of expansion α_T and the temperature T^* [see Eq. (7b)], and the sine of the angle θ that measures the inclination of the solar vector from the vertical; see Fig. 4. Recall that, for $\theta \leq 0$, the response is unconditionally stable. On the horizontal axis is the nondimensional parameter κ that is a ratio of the structural response time to the thermal response time. The three curves shown for the damping ratios $\zeta = 0.01, 0.001$, and 0.0001 are the stability boundaries. For a given damping ratio, designs below a stability boundary are stable, and designs above a stability boundary are unstable. The figure demonstrates that damping is a critical factor; increasing damping corresponds to a larger region of stable vibrations. Another critical parameter is the response time ratio κ. When $\kappa = 1$, the stability boundaries are at a minimum. Thus, a thermally induced vibration of a FRUSA solar array is more prone to be unstable when its thermal response time equals its structural response time.

To investigate the effects of boom parameters on the stability of the response, five booms that vary in radius and thickness were analyzed. These were selected from stainless steel BISTEMs manufactured by the Astro Corporation.[9] Table 2 lists the dimensions of five boom designs. These designs were selected because their critical buckling loads are larger than the HST solar blanket tension. Boom 4 is the HST design. The square symbols shown in Fig. 13 correspond to these designs for various values of the solar incident angle θ.

Stability of the five designs depends on the solar vector angle of incidence and the damping ratio. Since the solar arrays will nominally be facing the sun, the angle θ would typically be small, say $\theta < 10$ deg. Then the stability of the response is determined by the damping ratio. Under such conditions, all five designs including the HST are predicted to be stable for $\zeta \geq 0.1\%$ damping. However, for very small

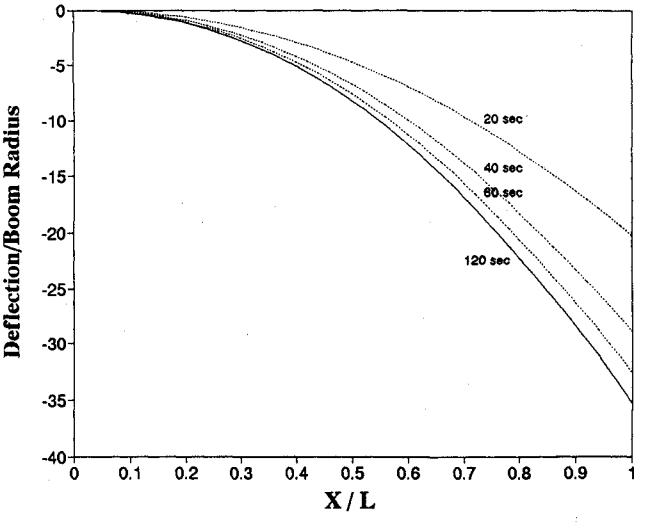

Fig. 11 Quasistatic deflection response of HST solar array.

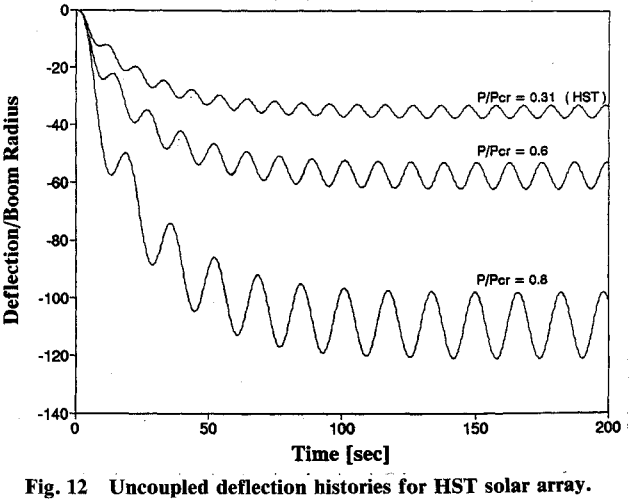

Fig. 12 Uncoupled deflection histories for HST solar array.

Table 2 Stainless steel booms

Boom	R, m	h, m
1	$3.962E-2$	$6.323E-4$
2	$2.540E-2$	$4.528E-4$
3	$1.702E-2$	$3.379E-4$
4 (HST)	$1.092E-2$	$2.351E-4$
5	$9.525E-3$	$1.811E-4$

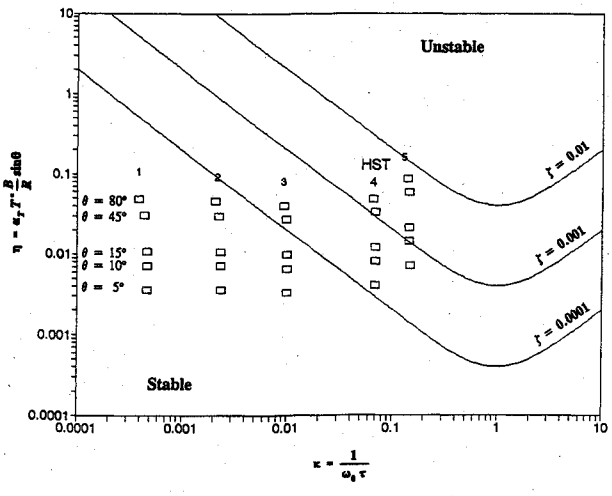

Fig. 13 Stability boundaries for HST solar array.

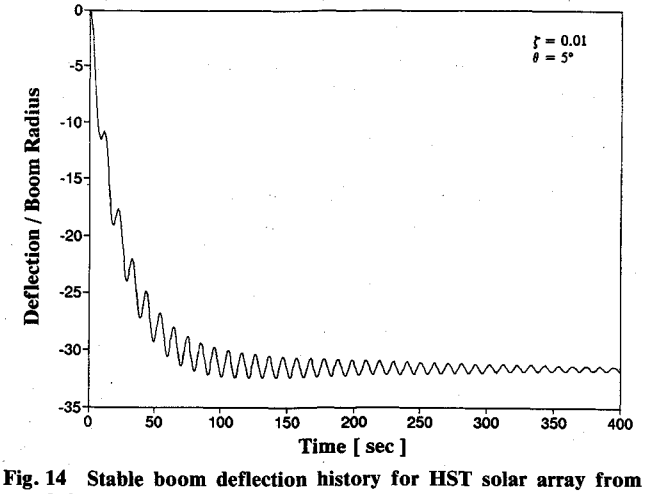

Fig. 14 Stable boom deflection history for HST solar array from coupled thermal-structural analysis.

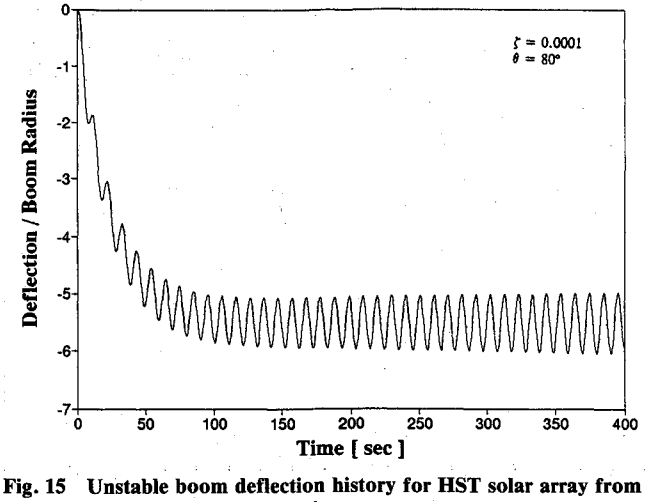

Fig. 15 Unstable boom deflection history for HST solar array from coupled thermal-structural analysis.

damping, say $\zeta = 0.01\%$, the HST design and design 5 are predicted to be unstable.

The analysis thus raises questions about the stability of thermally induced oscillations of the HST solar arrays. The analysis suggests the possibility of unstable oscillations, but a definitive conclusion cannot be reached without further knowledge of the in-orbit solar vector incident angle and the damping ratio.

Dynamic Response

The coupled dynamic response can be determined from the inverse Laplace transform of $U(s)$ in Eq. (35). To demonstrate the coupled thermal-structural responses, computations were performed for stable and unstable cases. Figure 14 presents a stable response for the HST solar array for a solar incident angle $\theta = 5$ deg and relatively high damping of $\zeta = 1\%$. The oscillation about the quasistatic deflection decays rapidly and oscillations would be negligible after about 6 min. In contrast, Fig. 15 presents an unstable response for the HST solar array for an incident angle $\theta = 80$ deg and relatively small damping of $\zeta = 0.01\%$. The stability analysis (see Fig. 13) predicts this case to be unstable, and indeed this is evident in the growing oscillations demonstrated in the dynamic response. Note that, because of the large incident angle, only a small component of the solar flux is absorbed by the boom, which results in the relatively small magnitude of the total response shown in Fig. 15.

The mechanism that causes the unstable oscillation is the time-dependent character of the incident normal heat flux. The time-varying angle between the incident solar vector and a normal to the beam surface determines the amount of flux absorbed by the beam. For $\theta > 0$, when the beam deforms toward the solar vector, the incident angle is reduced and more flux is absorbed. When the beam deforms away from the solar vector, the incident angle is increased and less flux is absorbed. This time-varying flux induces an oscillating temperature gradient that serves as a dynamic forcing function. The time-varying temperature gradient for the unstable oscillation is shown in Fig. 16. Although the amplitude of the temperature oscillation is small, it is increasing with time and coupled to the unstable displacement response of the boom.

The stability analysis showed that the HST solar array will experience unstable oscillation for $\theta = 5$ deg and $\zeta = 0.01\%$ damping. The dynamic response was predicted for these conditions and is shown in Fig. 17. Although the analysis predicts the response to be unstable, amplitude growth after 400 s is not discernable. In fact, the response was computed for greater than 4000 s (not shown), and the increase in vibration amplitudes was insignificant. The result shows for this solar inclination that unstable oscillations for the HST solar array are not of practical importance.

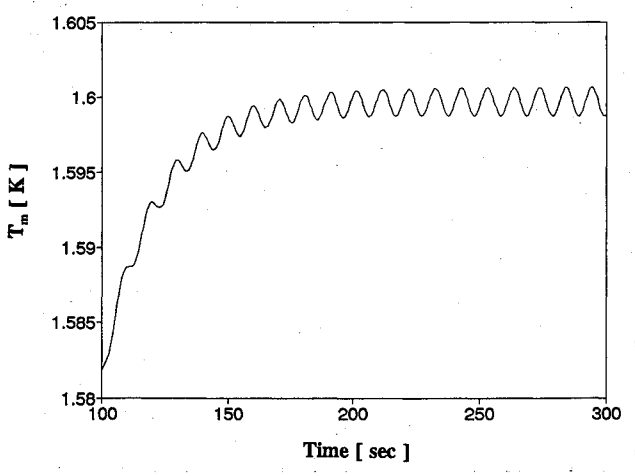

Fig. 16 Unstable perturbation temperature history for HST solar array from coupled thermal-structural analysis.

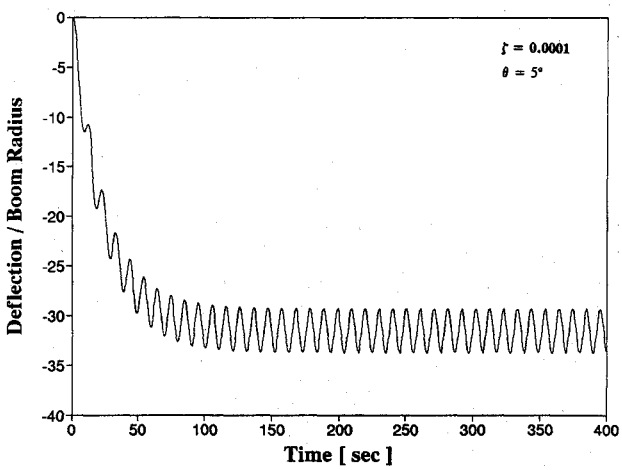

Fig. 17 Boom deflection history for HST solar array from coupled thermal-structural analysis.

Concluding Remarks

An analytical approach is developed for determining the thermal-structural response of a flexible rolled-up solar array due to a sudden increase in external heating. Two analyses are presented: 1) an uncoupled thermal-structural analysis that assumes the heating and temperature gradients are not affected by the thermally induced motions, and 2) a coupled thermal-structural analysis that includes the effects of structural deformations on heating and temperature gradients. In the first approach, the governing differential equations are solved analytically, and the dynamic response are determined by modal analysis. Equations are developed for the prediction of boom-buckling modes, solar array frequencies and mode shapes, thermally induced quasistatic deflections, and thermally induced vibrations. In the second approach, an approximate solution for the coupled thermal-structural response is obtained using the method of weighted residuals. A stability criterion and the dynamic response are obtained by Laplace transforms. A stability criterion given in nondimensional parameters establishes the conditions for which thermal flutter of the solar array may occur.

Numerical calculations are presented for the solar array design used on the Hubble Space Telescope. Thermally induced motions are caused by temperature gradients across the BISTEM booms. The analytical approach predicted a maximum temperature gradient of 20 K (36°F) that develops in about 120 s. Because of the temperature gradient, the 5.91 m (19.4 ft) booms experience a quasistatic tip deflection of about 0.38 m (15 in.). The uncoupled dynamic response predicted a thermally induced vibration at the first mode frequency of 0.097 Hz with an amplitude of 0.027 m (1 in.). The total dynamic response predicted is the sum of the quasistatic deflection and the superimposed thermally induced vibration. This response is fully developed after about 120 s.

Numerical calculations with the thermal flutter stability criterion raised questions about the stability of the thermally induced oscillations. The possibility of unstable oscillations was shown to exist and be strongly dependent on the inclination angle of the solar vector and system damping. For a solar vector inclination angle $\theta = 5$ deg, unstable oscillations could occur only for very small damping, say less than 0.01% equivalent viscous damping. Under these conditions, dynamic response calculations showed that the amplitude of the oscillations grows very slowly and are unlikely to have practical importance.

The analytical methods provide insight into the thermally induced behavior of a flexible rolled-up solar array and identify key parameters that are important for understanding the static and dynamic response. Such parameters include the thermal and surface properties of the boom material that determine the magnitude of the boom temperature gradient and the thermal response time. Significant structural parameters include the boom stiffness and thermal expansion coefficient that relate to the quasistatic deflection. Important also in the design is the boom compressive force that lowers the first mode natural frequency and affects the structural response time. Key parameters in determining the possibility of thermal flutter include the ratio of the thermal and structural response times, the solar inclination angle, and the system damping.

Acknowledgments

The research efforts of the authors were supported in part by the Light Thermal Structures Center established by a grant from the University of Virginia Academic Enhancement Program. The research of the second author was supported, in part, by a fellowship provided by the Virginia Space Grant Consortium.

References

[1]Thornton, E. A., and Foster, R. S., "Dynamic Response of Rapidly Heated Space Structures," *Computational Nonlinear Mechanics in Aerospace Engineering,* edited by S. N. Atluri, Vol. 146, Progress in Astronautics and Aeronautics, AIAA, Washington, DC, 1992, pp. 451–477.

[2]Graham, J. D., "Solar Induced Bending Vibrations of a Flexible Member," *AIAA Journal,* Vol. 8, No. 11, pp. 2031–2036.

[3]Rimrott, F. P. J., and Abdel-Sayed, R., "Flexural Thermal Flutter Under Laboratory Conditions," *Transactions of the Canadian Society for Mechanical Engineering,* Vol. 4, No. 4, 1976–77, pp. 189–196.

[4]Murozono, M., and Sumi, S., "Thermally Induced Bending Vibration of Thin-Walled Boom with Closed Section by Radiant Heating," *Memoirs of the Faculty of Engineering,* Kyushu Univ., Japan, Vol. 49, No. 4, 1989, pp. 273–290.

[5]Polidan, R. S., "Hubble Space Telescope Overview," AIAA Paper 91-0402, Jan. 1991.

[6]Foster, C. L., Tinker, M. L., Nurre, G. S., and Till, W. A., "The Solar Array-Induced Disturbance of the Hubble Space Telescope Pointing System," *Proceedings of the 61st Shock and Vibration Symposium* (Pasadena, CA), Vol. 4, Shock and Vibration Information Analysis Center, Arlington, VA, Oct. 1990, pp. 19–37.

[7]Boley, B. A., "Thermally Induced Vibrations of Beams," *Journal of the Aeronautical Sciences,* Vol. 3, No. 2, 1956, pp. 179–181.

[8]Reynolds, J., "The Analysis of the Deployed Space Telescope Solar Array," British Aerospace, ESA Document TN-SA-B142, Bristol, England, UK, Jan. 1983.

[9]Anon., "Stem Design Characteristics and Parameters," Astro Aerospace Corp., TR AAC-B-006, Carpinteria, CA, Sept. 1985.